Pattern formation on silicon by laser- initiated liquid-assisted colloidal lithography

M Ulmeanu1,6, P Petkov2, D Ursescu3,4, V A Maraloiu5, F Jipa3, E Brousseau2 and M N R Ashfold1
1 School of Chemistry, University of Bristol, Bristol BS8 1TS, UK
2 Cardiff School of Engineering, Cardiff University, Cardiff CF24 3AA, UK
3 National Institute for Laser, Plasma and Radiation Physics, Bucharest 077125 Romania
4 Extreme Light Infrastructure Nuclear Physics (ELI-NP)/Horia Hulubei National Institute for R and D in Physics and Nuclear Engineering (IFIN-HH), Bucharest 077125 Romania
5 National Institute for Material Physics, Bucharest 077125 Romania

Abstract

We report sub-diffraction limited patterning of Si substrate surfaces by laser-initiated liquid- assisted colloidal lithography. The technique involves exposing a two-dimensional lattice of transparent colloidal particles spin coated on the substrate of interest (here Si) immersed in a liquid (e.g. methanol, acetone, carbon tetrachloride, toluene) to a single picosecond pulse of ultraviolet laser radiation. Surface patterns formed using colloidal particles with different radii in the range 195 nm R 1.5 μm and liquids with differing indices of refraction (n_{liquid}) are demonstrated, the detailed topographies of which are sensitively dependent upon whether the index of refraction of the colloidal particle ($n_{colloid}$) is greater or smaller than n_{liquid} (i.e. upon whether the incident light converges or diverges upon interaction with the particle). The spatial intensity modulation formed by diffraction of the single laser pulse by the colloidal particles is imprinted into the Si substrate.

1. Introduction

Laser assisted surface patterning processes at the micro and nanoscale are important in a variety of applications. The possible consequences of laser irradiation can range from annealing of crystalline defects to material removal (ablation) or other non-ablative processes [1–3]. One of the major current challenges is to extend such laser-induced spatial and morphological changes from the micro to the nanoscale, which necessarily requires overcoming the diffraction limit barrier set by the wavelength of the light [4]. Optical near field technologies offer a way around this limitation, and potentially significant advances in material patterning and processing [5, 6]. One route to exploiting near field effects employs a self-assembled two-dimensional (2D) array of micron sized colloidal particles on a surface; laser irradiation through such an array in air promotes surface patterning by virtue of the enhanced electromagnetic field beneath each bead [7, 8]. The patterns observed when irradiating in air can be explained in terms of two limiting regimes: (a) when the bead radius R is much larger than the laser wavelength λ (R » λ), classical optics suffices, with the colloidal particle acting as a spherical lens that focusses the incident light directly beneath itself; and (b) when R «λ, the patterning can be described by Mie theory in the dipole approximation. Sub-diffraction limited focusing of the incident radiation is possible as near-field components of the electromagnetic field are still present [9]. 2D lattices of colloidal particles have also been used as arrays of microlenses on transparent supports [10]. These types of array can act like diffraction gratings, yielding significantly different interference patterns before and behind the focal plane [11]. Microlenses with different sizes, profiles, composition and indices of refraction have been investigated. The corresponding patterns produced in exposed and developed photoresist show feature dimensions as small as ∼100 nm [12], and topographies that are sensitive to the polarization, coherence and intensity distribution of the incident illumination. We have recently reported first illustrations of the laser-initiated, liquid-assisted colloidal (LILAC) lithography technique wherein irradiating the substrate of interest through an array of colloidal particles in different liquid media (rather than air) can yield a diverse range of surface patterns [13, 14]. The technique employs single pulse laser irradiation, together with self-assembled arrays of colloidal particles on a substrate (Si in the present case) immersed in a liquid. The choice of liquid defines the refractive index of the medium, and thereby offers a route to tuning the optical near-field effects around the colloidal particles. Here we report systematic studies of the ways in which the complex

surface patterns and topographies vary with the size and refractive index of the particles, the refractive index of the medium and the laser pulse energy. The results provide a much improved understanding of the diffraction phenomena observed with LILAC lithography methods, and open the way to the prediction and design of surface patterns with feature sizes below the diffraction limit.

2. Experimental section

The substrates were cut from n-type Si wafers (Crystal GmbH) and pre-treated in an oxygen plasma (Femto Diener, 80W power, 0.5 mbar O2 pressure) for 10 min to remove contaminants and render the surface hydrophilic. We assume bulk values for the optical constants of these Si substrates (i.e. n=5.61 and k=3.014 at λ=355 nm) [15]. Spherical colloidal particles, dispersed in water, were deposited on these substrates by spin coating [13]. Four types of particle were used in the present work: three sizes of silica particle, with respective radii R=1.5 μm, R=350 nm and R=195 nm (Bangs Laboratories) and one size of melamine particle with R=1.5 μm (Sigma Aldrich). The respective manufacturers quote refractive indices $n_{colloid}$=1.44 (silica) and $n_{colloid}$=1.68 (melamine), both measured at λ=589 nm. For the wavelength of current interest (λ=355 nm), $n_{colloid}$ (silica)=1.476 [16], while for melamine $n_{colloid}$ at λ=355 nm will be >1.68, but we have been unable to find a literature value for this quantity and henceforth continue to quote it as $n_{colloid}$=1.68. Laser irradiation of the colloidal particles spin coated onto the Si substrates was performed under four different liquids (volume∼1 cm^3, contained in an open trough of dimensions 25×25×20 mm^3), the refractive indices n_{liquid} of which are listed in table 1. The λ=589 nm data are from the literature [17, 18], and the corresponding n (λ=355 nm) values have been obtained by extrapolating the dispersion equations provided in these references. Attenuation of the incident laser radiation by the various solvents will be negligible, given their known absorption coefficients α(cm^{-1}) <0.04 at λ=355 nm [19]. Samples were irradiated with a Super Rapid diode pumped MOPA Nd:YVO4 laser (Lumera Lasers GMbh, 8 ps pulse duration, maximum output power 2W at λ=355 nm and a repetition rate of 10 kHz). The laser beam was controlled using WaveRunner software (Nutfield Technology) and a galvo scanner combined with a telecentric lens with focusing distance f=103 mm. The scan pattern was designed to ensure a series of equally spaced exposed areas on the substrate, each of which had been subject to a single shot of focussed (Gaussian spatial beam profile [14]) radiation from the laser operating at 10 kHz. Power levels used in the present work spanned the range 5≤P≤100 mW, which translate into incident fluences at the substrate surface in the range 0.28≤F≤5.66 J cm^{-2}. Sample characterization involved use of optical microscopy, scanning electron microscopy (JEOL IT300 SEM), atomic force microscopy (Bruker Multimode AFM) and high resolution (HR) transmission electron microscopy (JEOL JEM ARM200F TEM).

Table 1. Liquids used in the present LILAC lithography studies, together with their respective chemical formulae and refractive indices n_{liquid} (at λ = 589 nm and λ = 355 nm).

Liquid	Chemical formula	n_{liquid} (λ = 589 nm)	n_{liquid} (λ = 355 nm)
Methanol	CH_3OH	1.33	1.34
Acetone	CH_3COCH_3	1.36	1.37
Carbon tetrachloride	CCl_4	1.46	1.48
Toluene	$C_6H_5CH_3$	1.49	1.52

3. Results and discussion

The transparent colloidal spheres can cause incident illumination to converge or diverge depending on the sign of the difference between their refractive index ($n_{colloid}$) and that of the surrounding medium (n_{liquid}) [12]. Figures 1, 2 and 3 illustrate and compare the various possible lensing effects using geometrical optics (ray tracing), for the case when R»λ, and finite difference time domain (FDTD) simulations based on the Mie theory, for the case that R≤λ [20]. The wavelength (λ=355 nm) and particle refractive index ($n_{colloid}$=1.44) have been held fixed in these illustrative simulations, and the lensing properties tuned by varying the refractive index of the surrounding medium n_{liquid}. Figures 1 and 2 show calculated outputs for n_{liquid}=1.33 and n_{liquid}=1.49, respectively, with R=1.5 µm, while figure 3 shows calculated intensity distributions for these same two n_{liquid} values and for two different (small) particle radii (R=350 and 195 nm).

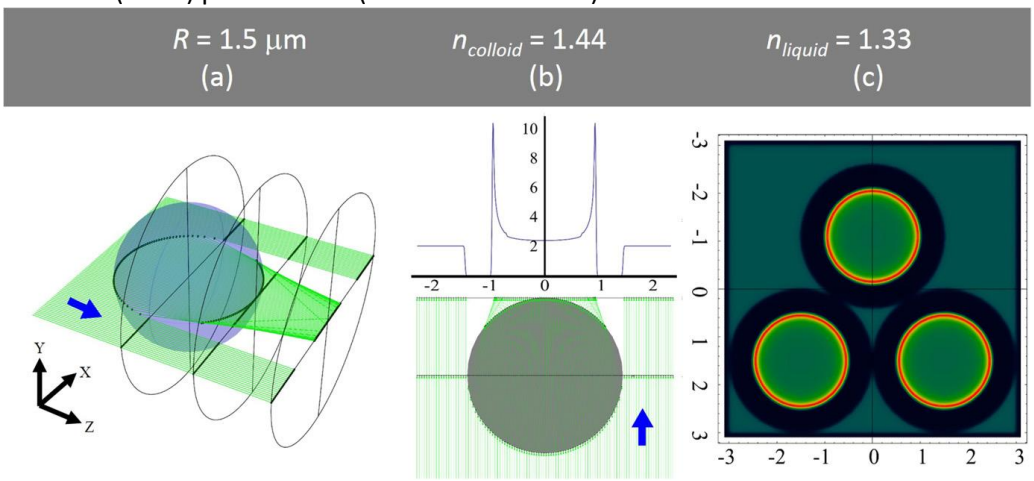

Figure 1. Ray tracing with collimated λ=355 nm light for (a) one sphere with R=1. 5 µm, $n_{colloid}$=1.44 and n_{liquid}=1.33, (b) the intensity distribution at the tangent surface derived from a 2D simulation using this one sphere and 1300 rays in the XZ plane, (c) false colour plot showing the light intensity distribution on the tangent surface under the spheres obtained with a 3D ray-tracing simulation for three contacting spheres.

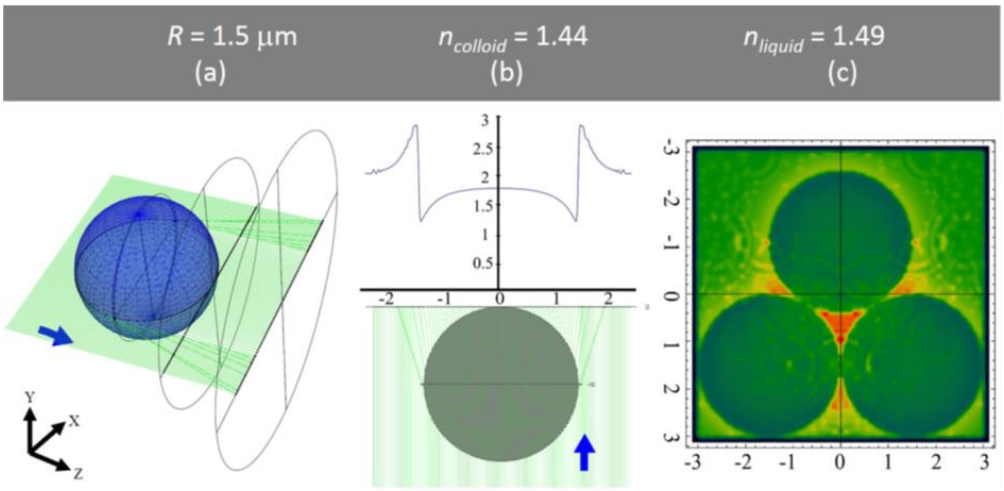

Figure 2. Ray tracing with collimated λ=355 nm light for: (a) one sphere with R=1. 5 µm, $n_{colloid}$=1.44 and n_{liquid}=1.49, (b) intensity distribution at the tangent surface derived from a 2D simulation using this one sphere and 1300 rays in the XZ plane, (c) false colour plot showing the light intensity distribution on the tangent surface under the spheres obtained with a 3D ray-tracing simulation for three contacting spheres.

Figures 1 and 2 show ray tracing simulations with collimated light (representing the confocal region of the laser beam) performed using the Optica3 software package for the Wolfram Mathematica programming environment, with the thick blue arrows indicating the direction of light propagation. These calculations do not allow for coherent interference or diffraction effects induced by the spheres. Figures 1(a) and (b) consider just a single sphere. The latter shows the intensity distribution at the tangent surface under the sphere, calculated using 1300 rays passing through the plane containing the centre of the sphere (i.e. a 2D calculation through the XZ plane defined in figure 1(a)), with the unperturbed incident laser intensity (I_0) set as 2. The false colour plot in figure 1(c) shows the intensity distribution at the surface for an arrangement of three contacting spheres, obtained from a full 3D simulation involving 123 904 uniformly distributed rays. The spacing between the source rays in the 3D simulation is 3.7-times greater, so the accuracy of the three particle simulation is lower, but the features evident from the 3D results (figure 1(c)) are consistent with the 2D benchmarking results shown in figure 1(b).
As figure 1 shows, high-index (i.e. $n_{colloid}>n_{liquid}$ spheres act as convergent lenses, forming a focal region on the tangent surface under the sphere characterized by increased intensity and a reduced spot diameter [12]. The most striking features, however, are the intense peaks at either edge of the focal region (in the 2D simulation, figure 1(b)), which map into an annular maximum in the 3D simulation (figure 1(c)). These arise from optical aberrations at the sides of the sphere and give rise to local intensities that are more than 5-times greater than I0. Beyond this ring, the shadow of the sphere on the tangent surface causes a region of zero intensity. All of these features are evident in the 3D three sphere simulation (figure 1(c)): the substrate surface at the interstice between the spheres is uniformly illuminated (at the incident intensity I0), intensity enhancement is observed within a circular focal region beneath the spheres, with the highest intensity appearing as a ring beyond which is an annulus of shadow extending out to the radius of the sphere.

A low-index ($n_{colloid}<n_{liquid}$) sphere, in contrast, acts as a divergent lens. The 2D ray tracing simulation in this case (figure 2(b)) shows an area on the tangent surface (with a radius slightly larger than that of the sphere itself) characterized by an incident intensity lower than I0 bounded by localized regions of minimal and maximal intensity; the latter feature maps into a ring (a 'halo') of enhanced intensity in the full 3D simulation (figure 2(c)). In contrast to the high-index $n_{colloid}>n_{liquid}$) case, the intensity modifications caused by a single low index sphere are mild; as figure 2(b) shows, relative to I0, the intensities at the tangent surface in the 'shadow' region under the sphere and in the 'halo' region beyond the edge of the sphere are only changed by, at most, ∼30% (reduction) and ∼50% (increase), respectively. Somewhat larger enhancements are achievable using arrays of low index spheres, however. As figure 2(c)) shows, the intensity at the tangent surface in the interstice between the spheres is ∼3- times greater than in the 'shadow' region. Nonetheless, relative to the high index spheres, the present simulations suggest that the incident laser intensity (relative to the substrate damage threshold) will be a more critical parameter when seeking a given surface pattern with LILAC lithography using low index spheres. We also note that ray tracing calculations for much smaller (R=350 nm) spheres yield results that are identical to those shown in figures 1(b) and 2(b) apart from the expected geometrical scaling factor.

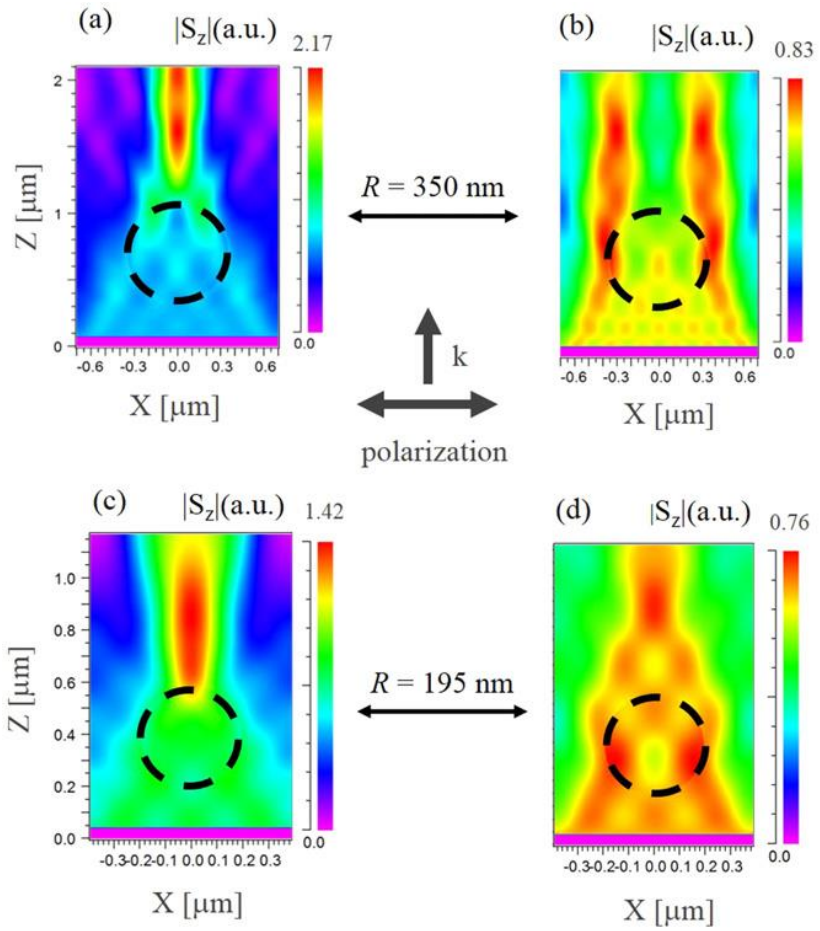

Figure 3. False colour plots showing the light intensity distributions returned by FDTD simulations for a single sphere with the following combinations of radius (r), $n_{colloid}$ and n_{liquid}: (a) 350 nm, 1.44, 1.33; (b) 350 nm, 1.44, 1.49, (c) 195 nm, 1.44, 1.33; (d) 195 nm, 1.44, 1.49. The black dashed lines show the position of the colloidal particle, and the linearly polarized (along X) incident radiation has wavelength λ=355 nm and propagates with wave vector k in the Z-direction.

Our previous FDTD simulations illustrated that the near field enhancement effects are also sensitive to the difference between n_{liquid} and $n_{colloid}$, and the substantial increases in the depth of focus that can be achieved in liquid assisted laser processing [14]. The false colour plots in figure 3 are the results of numerical Mie theory analysis using the Fullwave 9.1 software (RSoft Design). The simulation model comprises a single sphere with $n_{colloid}$=1.44, irradiated with linearly polarized (along X), 355 nm radiation propagating in the Z direction (starting to propagate from Z=2R/10) and the displayed electric field intensity distribution is perpendicular to the XZ plane. Figure 3 illustrates the magnitude of the Poynting vector for the Z direction $|S_z|$, defined as the directional energy flux per unit area in the vicinity of the colloidal particle (with $n_{colloid}$=1.44) in liquid media with n_{liquid}=1.33 (figures 3(a) and (c)) or n_{liquid}=1.49 (figures 3(b) and (d)). In each case, the two panels are for particles with R=350 nm and R=195 nm, respectively. These simulations highlight some of the changes in intensity distribution once R≤λ. The intensity patterns in the case that $n_{colloid}>n_{liquid}$ (figures 3(a) and (c)) are broadly similar to that reported previously for the case of a R=1.5 μm particle [14], but the region of maximum $|S_z|$ moves to progressively smaller Z/R with decreasing R. Conversely, in the case that $n_{colloid}<n_{liquid}$ (figures 3(b) and (d)), Mie scattering effects progressively dominate the 'defocusing' seen for larger particles (recall figure 2(b)) and, in the R=195 nm case, the maximum $|S_z|$ values are clearly under the sides of the particle. Nevertheless, the value of the $|S_z|$ for the low index regime is smaller than 1 (the value of $|S_z|$ when the field is propagating in free space, i.e. in

air). In this case, therefore, the presence of the colloidal particle causes no near-field enhancement and the electromagnetic field distribution is largely determined by Mie scattering effects [21]. The remainder of this paper reports experimental demonstrations of many of these predictions. A key parameter in designing surface patterns by LILAC lithography is the contrast between the refractive indices of the sphere and the liquid medium. Our previous study was restricted to particles of just one type and size size (silica, with R=1.5 μm) and a rather narrow range of $\Delta n=(n_{colloid}-n_{liquid})=-0.05$ to+0.11 [14]. Here we report results for a range of silica particle sizes (1.5 μm≥R≥195 nm) and for a wider range of refractive index differences ranging from Δn=−0.14 (in the case of silica beads in methanol) through to Δn=+0.35 through use of melamine ($n_{colloid}$=1.68) spheres with R=1.5 μm.

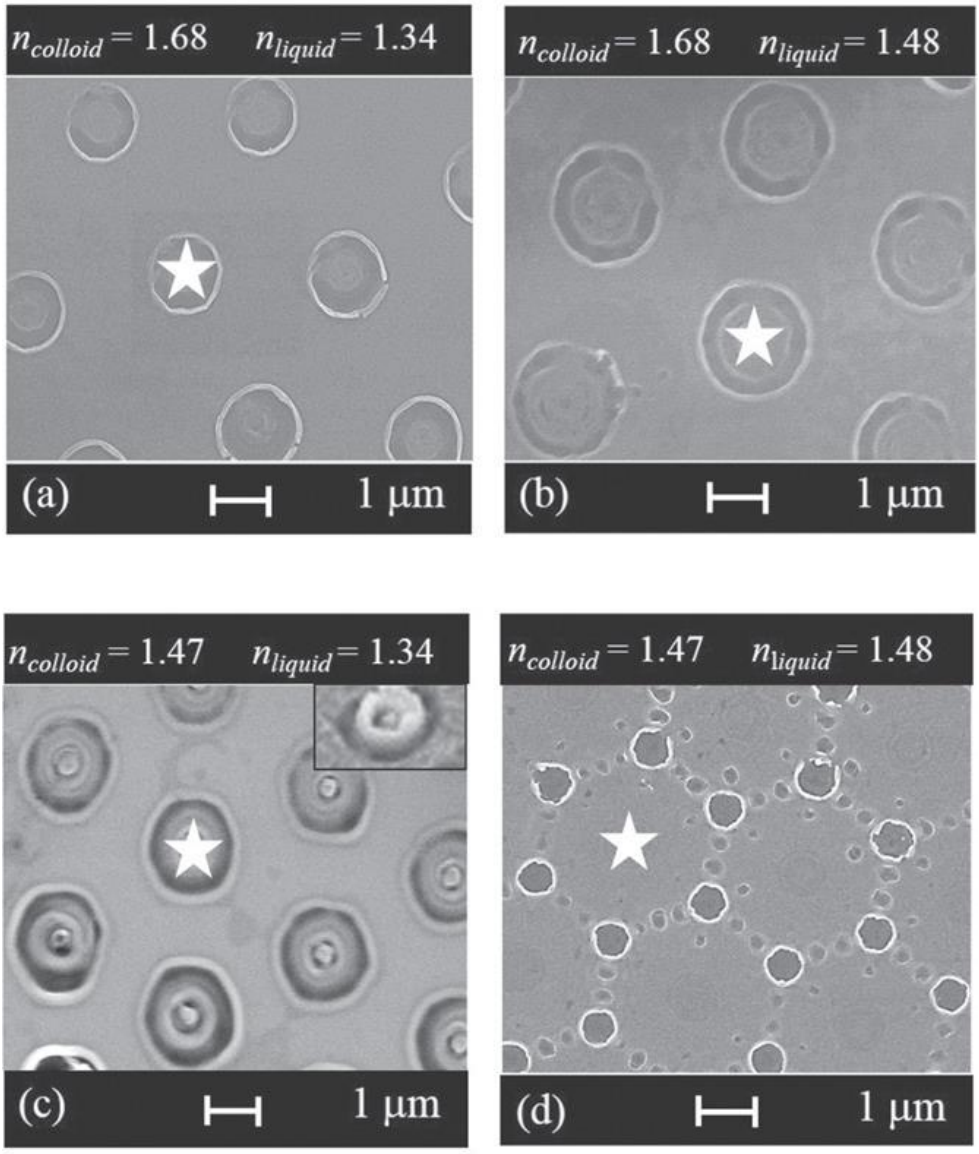

Figure 4. SEM images of the silicon substrate after irradiation with a single 355 nm laser pulse (F=2 J cm^{-2}) and the following R=1.5 μm colloidal particle/medium combinations: (a) melamine ($n_{colloid}$=1.68)/CH3OH (n_{liquid}=1.34); (b) melamine ($n_{colloid}$=1.68)/CCl4 (n_{liquid}=1.48); (c) silica ($n_{colloid}$=1.47)/CH3OH (n_{liquid}=1.34); (d) silica ($n_{colloid}$=1.47)/CCl4 (n_{liquid}=1.48). The AFM image shown as an inset in (c) illustrates the topography (a raised plug with a surrounding moat) of an individual imprinted structure.

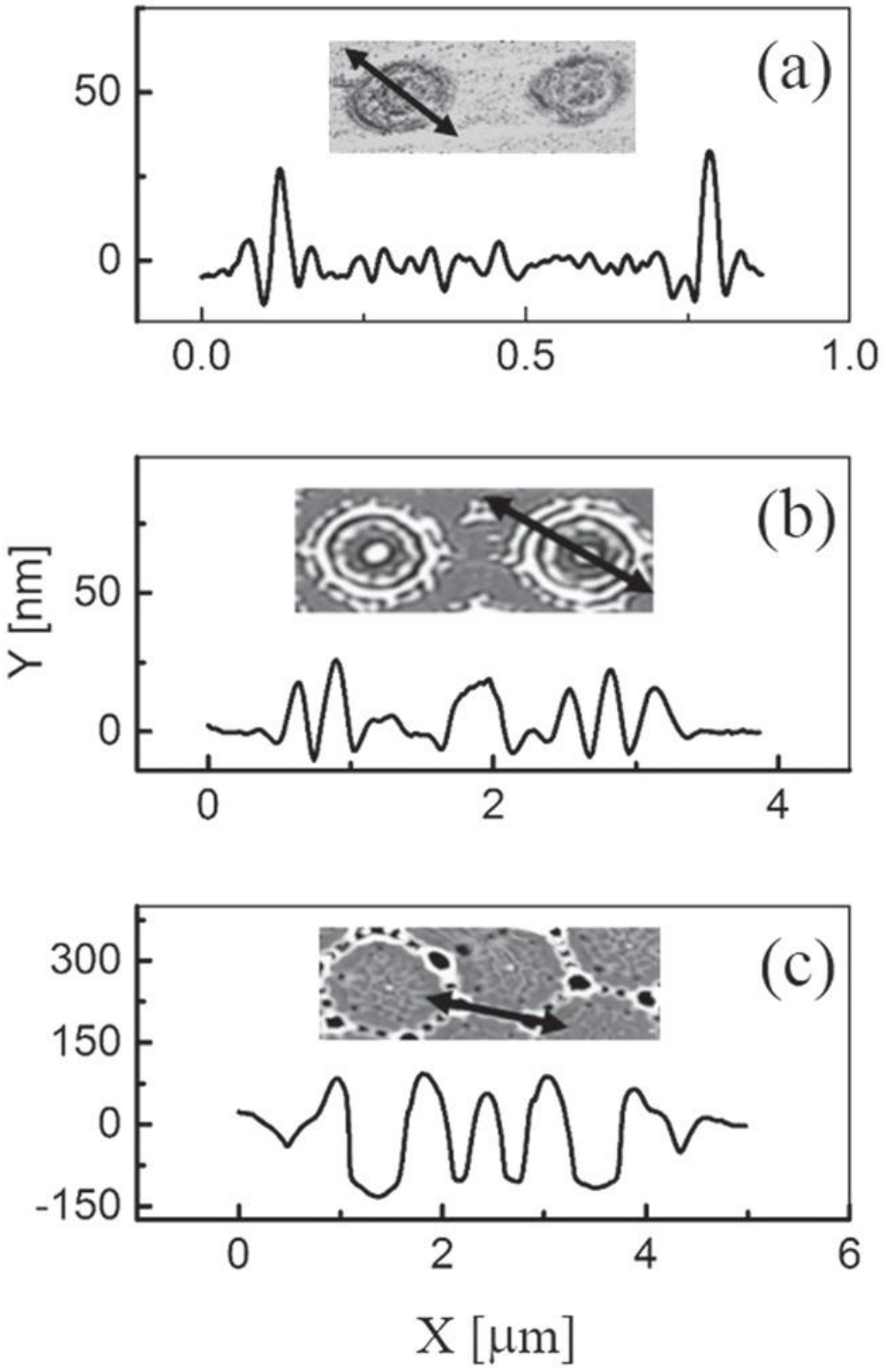

Figure 5. Line scans from the AFM images of Si surfaces patterned using LILAC lithography shown in the insets. The patterns were created using single pulses of 355 nm laser radiation (F=2 J cm^{-2}) and R=1.5 μm particles, with the following $n_{colloid}/n_{liquid}$ combinations: (a) 1.68/1.52; (b) 1.44/1.34; (c) 1.47/1.48.

Figures 4(a) and (b) show SEM images of patterns achieved by single pulse laser irradiation of a Si surface through a close packed monolayer of melamine particles immersed in liquids with n_{liquid}=1.34 and 1.48 with an incident fluence F=2 J cm^{-2}. The ray-tracing simulations corresponding to the melamine particles are qualitatively similar to those presented in figure 1, apart from the

obvious difference that the imprint created under the sphere is smaller (as expected, given the larger value of Δn), and in accord with the present experimental results. The white star in each panel in figure 4 indicates the centre location of one of the original particles, which are removed in the irradiated areas as a result of the recoil pressure accompanying the laser ablation [22]. Given that $n_{colloid} \gg n_{liquid}$, this is a high index regime, with a size parameter $\alpha = 2\pi R/\lambda = 17$, in which the colloidal particle acts as a micro-lens or micro-resonator [23, 24]. The diameter of the respective surface imprints increases from ∼1 μm (figure 4(a)) to ∼2 μm (figure 4(b)) as Δn decreases from 0.34 to 0.2, consistent with the expectation that these particles in these media act as converging lenses. Broadly analogous patterns are found using R=1.5 μm silica particles immersed in methanol (Δn=+0.13, figure 4(c)). Switching to a regime where $n_{colloid} < n_{liquid}$, however, as in the case of silica in carbon tetrachloride (Δn=−0.01, figure 4(d)), yields a very different pattern comprising a network of many small holes, with a range of diameters and a clear registration with the original particle locations. This is another important result. There is a wide and somewhat disparate literature pertaining to refractive values, and their variation with wavelength. Reference to table 1 shows that silica and CCl4 have very similar refractive indices at λ=355 nm, but the surface pattern shown in figure 4(d)leaves no doubt that this constitutes a low index regime (i.e.$n_{colloid} < n_{liquid}$), consistent with table 1.

Figure 5, which shows AFM data for selected imprints created using R=1.5 μm spheres in both low and high index regimes, provides further insights into the periodic patterns created by LILAC lithography. Clearly, the depth modulation created in these single shot irradiations is sufficient to give topographic contrast. In all cases, the Si surface structure resembles ripples on a liquid [25]. The periodicity and the position of the structures relative to the centre of the colloidal particle depend on the relative sign of Δn. Figures 5(a) and (b) serve to reinforce the finding that, under high index conditions (i.e. $n_{colloid} > n_{liquid}$), periodic rings develop in the area beneath the particle: the latter acts as a convergent lens. The line scan through the image shown in figure 5(b) shows that, under appropriate combinations of R and Δn, single shot laser processing can create localized 'humps' on the Si surface immediately beneath the particle centres. Figure 5(c) illustrates the other scenario, where $n_{colloid} < n_{liquid}$. Here the surface profiling is concentrated just outside the area eclipsed by the colloidal particle, i.e. the latter is acting as a divergent lens; the detailed form of the pattern around the edge of the eclipsed area can be understood as the superposition of two or three concentric annular rings originating from neighbouring particles. The laser induced holes in the Si surface shown in figure 5(c) exhibit depths in the range 40–130 nm and aspect (i.e. depth to width) ratios ranging from 0.15 to 0.35.

Figures 6 and 7 provide further illustrations of the diversity of the patterns achievable in the low index ($n_{colloid} < n_{liquid}$) regime. Panels 6(a) and (b) show SEM images of patterns obtained by irradiating through an array of R=1.5 μm silica ($n_{colloid}=1.47$) spheres immersed in toluene ($n_{liquid}=1.52$) at two different incident fluences, F=1 and 2 J cm^{-2}, respectively. The former image is noteworthy for two reasons. First, the irradiation occurred at the edge of the close packed array of particles and, second, F was insufficient to remove the particles. Figure 6(a) thus provides a particularly clear illustration of the concentric ripple structures emanating from a single particle (see the region bounded by the white box in the bottom right of the figure) and the formation of localized holes where the ripple patterns from multiple particles overlap and interfere. The depths and widths of the holes are sensitive to the order of the mutual interference of the rings (the largest holes are nearest the point of contact between neighbouring spheres in figure 6(a)), the number of interference rings (the largest holes are in regions that correspond to the interstices between the colloidal particles in figure 6(b)) and the incident fluence. At this point, we propose that the wave like structures arise as a result of diffraction of the laser beam on the colloidal particles, but further simulation work is needed for a quantitative understanding of the ways in which these particles scatter and focus the incident laser radiation. Figures 6(c) and (d) illustrate how the surface patterning can be varied by another user controllable parameter—the packing of the colloidal particles. These SEM images are of Si surfaces patterned using 355 nm laser pulses, F=2 J cm^{-2}, CCl_4 ($n_{liquid}=1.48$) as the liquid medium,

and a monolayer of R=1.5 µm silica particles in, respectively, hexagonal close packed (hcp) and body centre cubic arrangements. The areas bounded by the white lines are all relative depressions. The SEM images presented in figure 7 illustrate how particle size affects the surface patterning by single shot irradiation of hcp arrays of silica particles immersed in CCl4 at an incident fluence F=4 J cm^{-2}. The pattern obtained with R=1.5 µm spheres (figure 7(a)) is sensibly consistent with that shown in figure 6(c). The hexagonal motif is still clearly evident in the pattern formed with R=350 nm particles (figure 7(b)), but the relative depth and width of the holes formed by the interfering ripple structures are increased. This trend is continued upon further reduction in particle size, to R=195 nm (figure 7(c)), where the SEM image shows a rather uniform ablation 'moat' around the original site of each particle and a yet more developed 'hump' under the original particle centre. All of these observations are broadly consistent with previous suggestions that irradiation promotes a capillary wave with a wavelength that is dependent on Δn, R and λ [26].

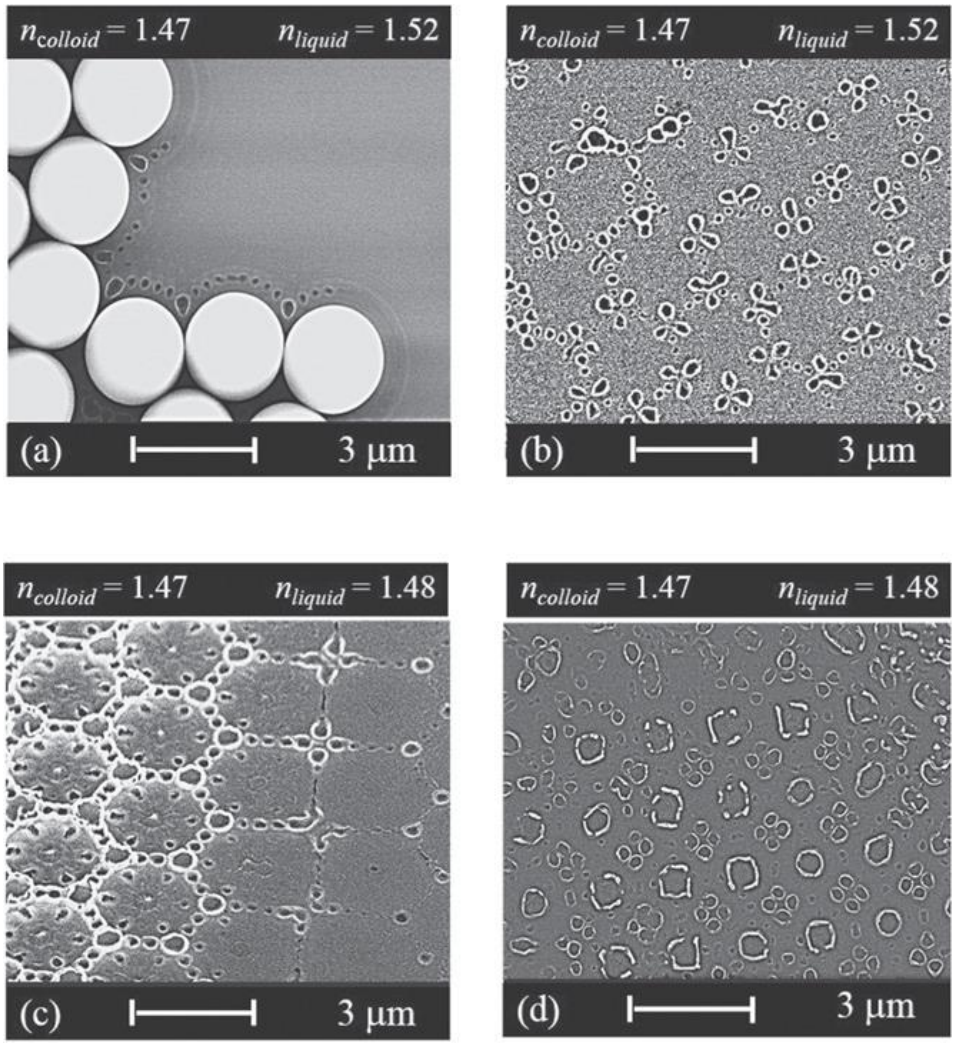

Figure 6. SEM images of surface patterns formed by LILAC lithography using R=1.5 µm spheres in the low index ($n_{colloid}<n_{liquid}$) regime: (a) and (b) Δn=−0.05, and F=1 and 2 J cm^{-2}, respectively; (c) and (d) Δn=−0.01, with, respectively, hexagonal and body centre cubic close packed arrangements of the colloidal particles.

Figure 8 shows SEM images illustrating the variation in surface patterning with change in particle size when irradiating at F=4 J cm^{-2} in the high index ($n_{colloid}>n_{liquid}$) regime, using silica particles in methanol. The pattern formed using the R=1.5 µm particles is reminiscent of that found at lower F

(figure 4(c)), with concentric ripple structures beneath the locus of each particle but also shows evidence of patterning around the periphery of each particle. This pattern evolves upon reducing R such that, by R=195 nm (figure 8(c)), the surface pattern is dominated by an hcp array of 'humps' (height~40 nm, FWHM~120 nm) with a registration that matches that of the colloidal particles used for the LILAC processing.

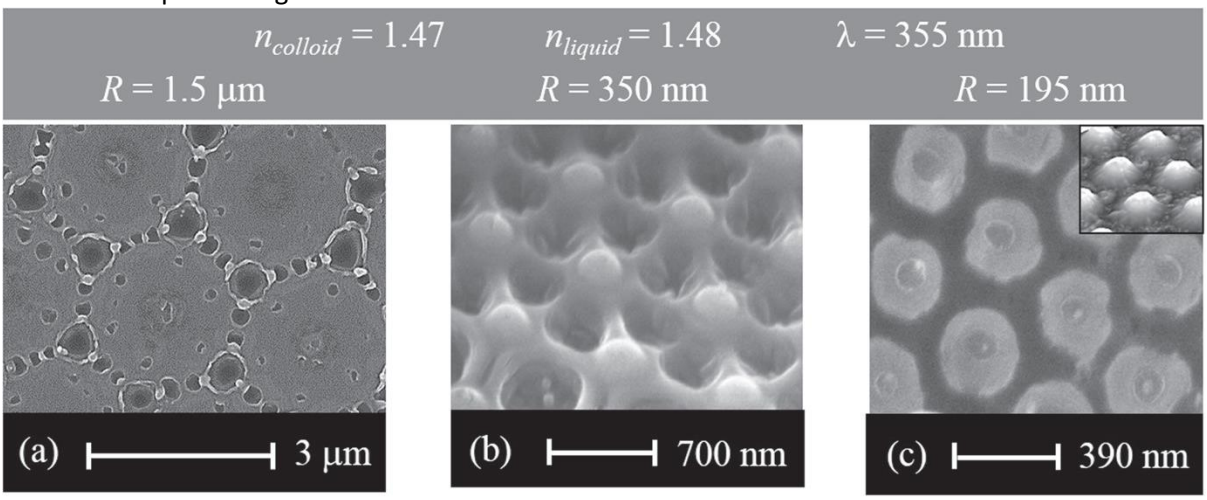

Figure 7. SEM images of Si substrates patterned using a single pulse of 355 nm radiation (F=4 J cm^{-2}), CCl4 (n_{liquid}=1.48) as the liquid medium and silica particles ($n_{colloid}$=1.47) with R=(a) 1.5 μm, (b) 350 nm and (c) 195 nm (the AFM image included as an inset within panel (c) provides a further illustration of the surface topography, with obvious humps separated by ~390 nm under the centre of each particle site.).

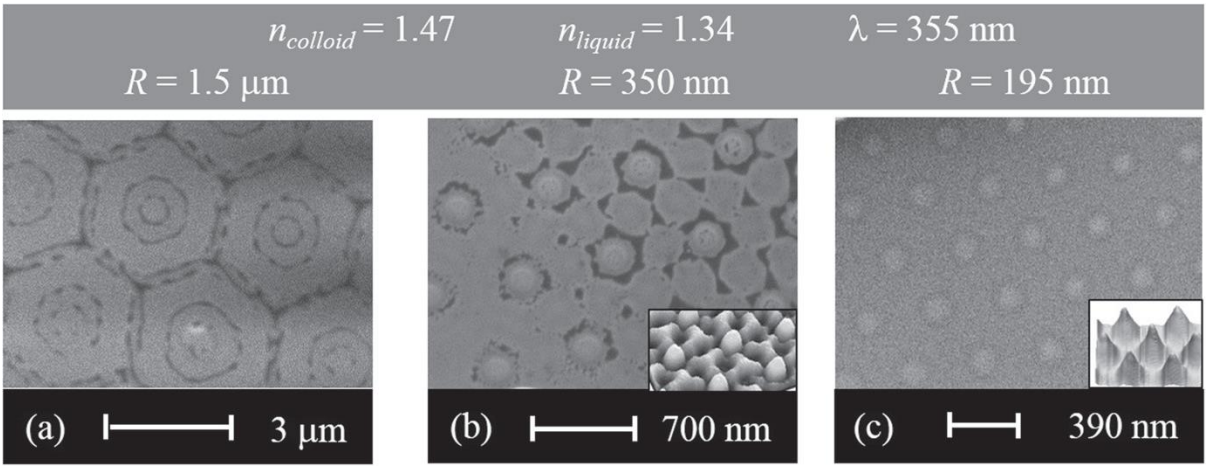

Figure 8. SEM images of Si substrates patterned using a single pulse of 355 nm radiation (F=4 J cm^{-2}), methanol (n_{liquid}=1.34) as the liquid medium and silica particles ($n_{colloid}$=1.47) with R=(a) 1.5 μm, (b) 350 nm and (c) 195 nm. AFM images of localized regions of the patterned surface are shown as insets in (b) and (c).

Individual hump structures in the patterned Si sample shown in figure 8(b) were investigated by conventional and HR TEM. One hump and part of the underlying substrate are evident in the conventional cross-sectional TEM image (60 000× magnification) of a thinned sample shown in Figure 9(a). LILAC processing has clearly modified the surface (cf unirradiated regions where the surface is smooth as in other regions without deposition, but energy dispersive x-ray (EDX) spectra taken from localized (~2 nm diameter) regions within the hump and substrate regions indicate the same chemical composition (i.e. SiKα peak only). The HRTEM image (figure 9(b), 600 000× magnification) taken at the hump-substrate interface shows obvious fringes, but no obvious epitaxy

between the substrate and the hump; fast Fourier transforms (FFTs) of the structure evident in selected regions of the image confirm the polycrystalline nature of the Si in the hump.

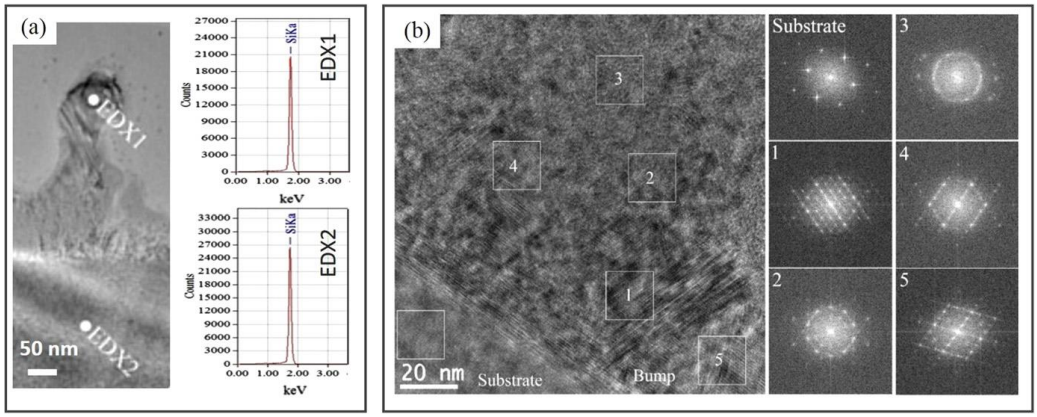

Figure 9. (a) Conventional cross-sectional TEM image of a hump on a LILAC processed Si substrate, along with EDX spectra taken from the indicated regions within the hump and the substrate. (b) HRTEM image taken at the substrate–hump interface along with FFTs of the patterns observed in six regions of the image.

4. Conclusion

This study demonstrates the formation of regular micron and submicron-size patterns on Si substrates by LILAC lithography. The surface patterns derive from concentric rings that originate from beneath the centre of each particle in the irradiated array, but the detailed form of these rings and their mutual interference is shown to be sensitively dependent on the difference in the refractive index of the particles (ncolloid) and the liquid medium (nliquid) in which they are immersed, and the particle size. The ripple-like surface structures are tentatively ascribed to diffraction of the laser beam on the colloidal particles, but further experiments and simulations are currently underway to provide a fuller understanding of the ways in which incident radiation is scattered and focused by interaction with colloidal particles immersed in different liquid media.

Acknowledgments

MU is supported by a Marie Curie International Intra-European Fellowship, Research Executive Agency (FP7-PEOPLE-2013-IEF-625403). PP acknowledges the support of the Interreg IVB project ‘ECO-efficient LASER technology for FACTories of the future’. MNRA acknowledges support from the Engineering and Physical Sciences Research Council(EPSRC, EP/K018388/1). The SEM/AFM studies were carried out in the Chemical Imaging Facility, University of Bristol with equipment funded by EPSRC under Grant ‘Atoms to Applications’ (EP/K035746/1).

References

[1] Im J S, Kim H J and Thompson M O 1993 Phase transformation mechanisms involved in excimer laser crystallization of amorphous silicon films Appl. Phys. Lett. 63 1969–71
[2] Cavalleri A, Sokolowski-Tinten K, Bialkowski J, Schreiner M and von der Linde D 1999 Femtosecond melting and ablation of semiconductors studied with time of flight mass spectroscopy J. Appl. Phys. 85 3301–9
[3] Farrokhi H, Zhou W, Zheng H Y and Li Z L 2012 Nonablative texturing of silicon surface with a continuous wave fiber laser Opt. Express 20 23180–5
[4] Zheludev N I 2008 What diffraction limit? Nat. Mater. 7420–2
[5] McLeod E and Arnold C B 2008 Subwavelength direct-write nanopatterning using optically trapped microspheres Nat.Nanotechnology 3 413–7
[6] Martin-Fabiani I, Siegel J, Riedel S, Boneberg J, Ezquerra T A and Nogales A 2013 Nanostructuring thin polymer films with optical near fields ACS Appl. Mater. Interfaces 5 11402–8

[7] Brodoceanu D, Landstrom L and Bauerle D 2007 Laserinduced nanopatterning of silicon with colloidal monolayers Appl. Phys. A 86 313–4
[8] Wang Z B, Joseph N, Li L and Luk'yanchuk B S 2010 A review of optical near-fields in particle/tip-assisted laser nanofabrication Proc. Inst. Mech. Eng. 224 1113–27
[9] van de Hulst H C 1981 Light Scattering by Small Particles (New York: Dover)
[10] Bauerle D, Piglmayer K, Denk R and Arnold N 2002 Laser induced surface patterning by means of microspheres Appl. Phys. Lett. 80 4693–5
[11] Denk R, Piglmayer K and Bauerle D 2003 Laser-induced nanopatterning by means of interference subpatterns generated by microspheres Appl. Phys. A 76 1–3
[12] Wu M H, Paul K E and Whitesides G 2002 Patterning flood illumination with microlens arrays Appl. Opt. 412575–85
[13] Ulmeanu M, Petkov P, Hirshy H and Brousseau E 2014 Formation of ordered arrays of Si and GaAs nanostructures by single-shot laser irradiation in near-field at the solid/liquid interface Mater. Res. Express 1 015030–9
[14] Ulmeanu M, Grubb M P, Jipa F, Quignon B and Ashfold M N R 2015 3D patterning of silicon by laser initiated, liquid-assisted colloidal (LILAC) lithography, J. Colloid Interface Sci. 447 258–62
[15] Palik E D 1988 Handbook of Optical Constants of Solids (New York: Academic)
[16] Malitson I H 1965 Interspecimen comparison of the refractive index of fused silica J. Opt. Soc. Am. 55 1205–9
[17] Moutzouris K, Papamichael M, Betsis S C, Stavrakas I, Hloupis G and Triantis D 2014 Refractive, dispersive and thermo-optic properties of twelve organic solvents in the visible and near-infrared Appl. Phys. B 116617–22
[18] Rheims J, Koser J and Wriedt T 1997 Refractive-index measurements in the near-IR using an Abbe refractometer Meas. Sci. Technol. 8 601–5[19] Duley W W 2005 UV Lasers: Effects and Applications inMaterial Science (Cambridge: Cambridge University Press)
[20] Mie G 1908 Beiträge zur Optik trüber Medien, speziell kolloidaler Metallösungen Ann. Phys. Lpz. 330 377–445
[21] Sakai T, Miyanishi T, Nedyalkov N, Nishizawa Y and Obara M 2009 Nano-dimple processing of silicon surfaces by femtosecond laser irradiation with dielectric particle templates in the Mie scattering domain J. Phys. D: Appl. Phys. 42 025502
[22] Fourrier T, Schrems G, Muehlberger T, Heitz J, Arnold N,Bauerle D, Mosbacher M, Boneberg J and Leiderer P 2001 Laser cleaning of polymer surfaces Appl. Phys. A 72 1–6
[23] Owen J F, Chang R K and Barber P W 1981 Internal electric field distributions of a dielectric cylinder at resonance wavelengths Opt. Lett. 6 540–2
[24] Benincasa D S, Barber P W, Zhang J Z, Hsieh W F and Chang R K 1987 Spatial distribution of the internal and near-field intensities of large cylindrical and spherical scatterers Appl. Opt. 26 1348–56
[25] Shen M Y, Crouch C H, Carey J E and Mazur E 2004 Femtosecond laser-induced formation of submicrometer spikes on silicon in water Appl. Phys. Lett. 85 5694–6
[26] Shen M Y, Crouch C H, Carey J E, Younkin R, Mazur E, Sheehy M and Friend C M 2003 Formation of regular arrays of silicon microspikes by femtosecond laser irradiation through a mask Appl. Phys. Lett. 82 1715–7